

Sidebands in the light absorption of driven metallic nanoparticles

G. Weick^{1,2,3,a}, G.-L. Ingold², D. Weinmann¹, and R.A. Jalabert^{1,2}

¹ Institut de Physique et Chimie des Matériaux de Strasbourg, UMR 7504 (ULP-CNRS), 23 rue du Loess, BP 43, 67034 Strasbourg Cedex 2, France

² Institut für Physik, Universität Augsburg, Universitätsstraße 1, 86135 Augsburg, Germany

³ Fachbereich Physik, Freie Universität Berlin, Arnimallee 14, 14195 Berlin, Germany

Received 28 March 2007

Published online 20 June 2007 – © EDP Sciences, Società Italiana di Fisica, Springer-Verlag 2007

Abstract. The dynamics of the surface plasmon in laser-driven metallic nanoparticles is described by means of a master-equation formalism. Within the Markov approximation, the dynamics is studied for different regimes ranging from weak excitation in photoabsorption experiments to strong excitation in pump-probe spectroscopy. It is shown that two collective levels are sufficient to describe the dynamics of the surface plasmon. On this basis, we predict the appearance of sidebands in the absorption spectrum of the probe laser field in pump-probe experiments.

PACS. 78.67.Bf Nanocrystals and nanoparticles – 73.20.Mf Collective excitations – 71.45.Gm Exchange, correlation, dielectric and magnetic response functions, plasmons

1 Introduction

A surface plasmon excited by a pump laser in a metallic nanoparticle decays on the scale of tens of femtoseconds by heating the electron system [1,2]. The equilibration with the ionic lattice occurs on the much longer timescale of a few picoseconds. This electronic relaxation has been thoroughly studied by means of pump-probe experiments [3–6]. Present femtosecond resolution experiments allow to concentrate on the initial dynamics of the electronic degrees of freedom [7–9]. While the dynamics on the picosecond scale has been analysed with quasi-equilibrium theories assuming the thermalisation of the electron gas as a whole [10], much less is known for the initial dynamics. It is precisely this initial regime on which we focus in this work.

For the description of the initial dynamics of the electron gas, before it has thermalised after an excitation by a laser pulse, it is appropriate to decompose the electron system into two parts [11–13]. The main degree of freedom describes the surface plasmon and refers to the centre of mass of the electron gas. The remaining degrees of freedom consist of the relative coordinates. If their number is sufficiently large, this electronic subsystem behaves to a good approximation as a heat bath to which one can attribute an effective temperature.

The surface plasmon coupled to the relative coordinates and driven by an external field is reminiscent of the situation encountered in quantum optics, where a laser-driven atom is coupled to an environment consisting of

the electromagnetic field modes [14]. This analogy leads us to predict the appearance of sidebands in the light absorption of a weak probe beam while the nanoparticle is illuminated by a strong pump laser. This effect should be experimentally observable and offers a possibility to study the surface plasmon dressed by photons of the pump laser field.

We start in the next section by introducing the model of a laser-driven nanoparticle. In Section 3, a master-equation description for the dynamics of the electronic centre of mass coupled to the relative-coordinate system is developed. We will argue that the Markov approximation applies in our situation. In order to make progress, we restrict in Section 4 our description of the surface plasmon to its two lowest eigenstates and discuss the resulting dynamics. The regime of validity of the two-level approximation will be discussed in the appendix. In Section 5, the model parameters for typical experimental situations are estimated. Finally, we present in Section 6 our prediction of sidebands in the absorption spectrum of a weak probe beam impinging on a nanoparticle subject to a pump laser.

2 Model of a laser-driven nanoparticle

The electron gas formed by the N valence electrons of the metallic nanoparticle is described by the Hamiltonian

$$H = \sum_{i=1}^N \left[\frac{p_i^2}{2m_e} + U(|\mathbf{r}_i|) \right] + \frac{e^2}{2} \sum_{\substack{i,j=1 \\ (i \neq j)}}^N \frac{1}{|\mathbf{r}_i - \mathbf{r}_j|}, \quad (1)$$

^a e-mail: weick@physik.fu-berlin.de

where \mathbf{r}_i is the position of the i th electron. The single-particle confining potential U represents the interaction of the electrons with the ionic background which within the jellium model is approximated by a uniformly charged sphere of radius a [2]. As a function of the radial coordinate, this central potential is harmonic for $|\mathbf{r}| < a$ and Coulomb-like for $|\mathbf{r}| > a$.

For our purposes it is useful to express the Hamiltonian (1) in terms of the centre-of-mass and relative coordinates as [11, 13]

$$H = H_{\text{cm}} + H_{\text{rel}} + H_c. \quad (2)$$

For small centre-of-mass displacements, H_{cm} is well described in terms of the usual ladder operators b^\dagger and b by the harmonic oscillator Hamiltonian

$$H_{\text{cm}} = \hbar\tilde{\omega}_M b^\dagger b \quad (3)$$

with a frequency

$$\tilde{\omega}_M = \omega_M \sqrt{1 - \frac{N_{\text{out}}}{N}}. \quad (4)$$

Here, $\omega_M = (4\pi n_e e^2 / 3m_e)^{1/2}$ is the classical Mie frequency which depends on the charge e , the mass m_e and the bulk density n_e of the electrons. The spill-out effect [2], which accounts for the fact that a fraction N_{out}/N is found outside the nanoparticle, reduces the electron density and thus leads to a redshift of the plasmon frequency from the Mie frequency to $\tilde{\omega}_M$. Except for extremely small clusters, anharmonicities yield negligible corrections to (3) and are thus disregarded here [15].

Within the mean-field approximation, the Hamiltonian for the relative coordinates reads

$$H_{\text{rel}} = \sum_{\alpha} \varepsilon_{\alpha} c_{\alpha}^{\dagger} c_{\alpha}, \quad (5)$$

where ε_{α} are the eigenenergies in the effective mean-field potential V and c_{α}^{\dagger} (c_{α}) are the creation (annihilation) operators associated with the corresponding one-body eigenstates $|\alpha\rangle$. Numerical calculations within the local density approximation show that, for the purpose of analytical calculations, V can in general be approximated by a step-like potential at the surface of the nanoparticle [12, 13].

The linearised coupling Hamiltonian between the centre-of-mass and relative-coordinate systems can be written as

$$H_c = \Lambda (b^\dagger + b) \sum_{\alpha\beta} d_{\alpha\beta} c_{\alpha}^{\dagger} c_{\beta}, \quad (6)$$

where the coupling strength $\Lambda = (\hbar m_e \omega_M^3 / 2N)^{1/2}$. The matrix element $d_{\alpha\beta}$ between two eigenstates of the unperturbed mean-field problem appearing in (6) is for a spherical hard-wall potential simply given by the dipole matrix element $\langle \alpha | z | \beta \rangle$ [12]. Here, we have assumed that the surface plasmon oscillates in the z direction. The sum of (6) has to be understood with a low-energy cutoff since the electron-hole excitations of low energy do not couple to the surface plasmon [13, 16]. This cutoff energy has been

estimated in [17] to be of the order of 3/5 of the Fermi energy for the case of Na nanoparticles.

The decomposition (2) is reminiscent of the well-studied case where the degree of freedom of interest (the surface plasmon in our case) is weakly coupled to a reservoir with many degrees of freedom (the relative coordinates). Interestingly, it can be shown that it is sufficient to have about $N = 20$ conduction electrons to define a proper environment for the surface plasmon [17]. Since the electronic system is coupled to phonons, a time dependence of the electronic temperature T may have to be taken into account. However, the physical parameters describing the dynamics of the surface plasmon are only weakly temperature dependent [13], and thus we can neglect the implicit time dependence of those parameters when T is much smaller than the Fermi temperature of the system.

If the nanoparticle is subject to a laser excitation, we have to add the coupling $H_F(t)$ between the electrons and the laser field to the Hamiltonian (2). Excitation frequencies ω_L close to the plasmon resonance are located in the visible range, and therefore the electromagnetic field has a wavelength much larger than the size of the nanoparticle. This external electrical field can be considered as spatially homogeneous, $\mathbf{E}(t) = E_0 \cos(\omega_L t) \mathbf{e}_z$, and thus it only couples to the electronic centre of mass. In the dipolar approximation, the interaction between the driving field and the centre-of-mass system reads

$$H_F(t) = (b^\dagger + b) \hbar \Omega_R \cos(\omega_L t). \quad (7)$$

The Rabi frequency Ω_R is given by

$$\hbar \Omega_R = e E_0 N \ell, \quad (8)$$

where

$$\ell = \sqrt{\frac{\hbar}{2N m_e \tilde{\omega}_M}} \quad (9)$$

is the characteristic length associated with the harmonic oscillator (3).

Different physical regimes can be attained according to the relative values of the typical energies $\hbar\omega_M$, $a\Lambda$, $\hbar\Omega_R$, and the Fermi energy of the metal.

3 Centre-of-mass density matrix

In the first part of this section we consider the free evolution of the centre of mass without the external driving field. The driving term (7) will be added in the second part.

3.1 Free evolution of the centre of mass

The evolution of the whole system in the absence of the electromagnetic field ($H_F = 0$) can be expressed in terms of the total density matrix $W(t)$. Assuming that the coupling (6) is a small perturbation, we write the time evolution of the density matrix as

$$\dot{W}(t) = -\frac{i}{\hbar} \left[\tilde{H}_c(t), \tilde{W}(t) \right], \quad (10)$$

where the tilde denotes operators in the interaction picture with respect to the uncoupled Hamiltonian $H_{\text{cm}} + H_{\text{rel}}$.

As we are only interested in the dynamics of the centre of mass, we trace out the relative coordinates to obtain the reduced density matrix $\rho = \text{Tr}_{\text{rel}} W$ which obeys the equation of motion

$$\begin{aligned} \dot{\rho}(t) = & -\frac{i}{\hbar} \text{Tr}_{\text{rel}} \left[\tilde{H}_c(t), W(0) \right] \\ & - \frac{1}{\hbar^2} \int_0^t ds \text{Tr}_{\text{rel}} \left[\tilde{H}_c(t), \left[\tilde{H}_c(s), \tilde{W}(s) \right] \right]. \end{aligned} \quad (11)$$

In dissipative quantum dynamics the environment is thought of as being infinite and remaining in thermal equilibrium at all times, i.e., its intrinsic properties like the temperature do not change as a consequence of its coupling to the system [18]. In order to satisfy this condition, we have to assume that the internal equilibration of the relative degrees of freedom after an excitation occurs sufficiently fast. This last assumption is not equivalent to the thermalisation of the whole electron gas, which can only occur when the plasmon has decayed. The internal thermalisation hypothesis can be justified a posteriori by checking that the timescale of the temperature change of the relative degrees of freedom is larger than all the other relevant timescales.

Restricting ourselves to the lowest order in the correlations between system and environment in (11), the weak coupling limit that we assume to be valid allows to write (for details, see Chap. 4 in [14])

$$W(t) \approx \rho(t) \otimes \rho_{\text{rel}} \quad (12)$$

at any time $t \geq 0$. Here,

$$\rho_{\text{rel}} = \frac{e^{-\beta(H_{\text{rel}} - \mu N)}}{\Xi} \quad (13)$$

represents the density matrix of the environment in the grand-canonical ensemble, i.e., we ignore for this purpose the finite nature of the electron gas. Ξ is the grand-canonical partition function at the inverse temperature $\beta = (k_{\text{B}}T)^{-1}$ and μ is the chemical potential.

As a consequence of the structure of the coupling H_c , the fact that $d_{\alpha\alpha} = 0$ due to the dipole selection rules [12], and the assumption of a factorising initial condition, the first term on the right-hand side of (11) vanishes. With the weak-coupling limit, (11) then reads

$$\dot{\rho}(t) \simeq -\frac{1}{\hbar^2} \int_0^t ds \text{Tr}_{\text{rel}} \left[\tilde{H}_c(t), \left[\tilde{H}_c(s), \tilde{\rho}(s) \otimes \rho_{\text{rel}} \right] \right]. \quad (14)$$

The trace over the electronic environment (5) yields

$$\begin{aligned} \dot{\rho}(t) = & \frac{1}{\hbar^2} \int_0^t d\tau C(\tau) \\ & \times \left[\tilde{b}^\dagger(t) + \tilde{b}(t), \tilde{\rho}(t-\tau) \left(\tilde{b}^\dagger(t-\tau) + \tilde{b}(t-\tau) \right) \right] + h.c. \end{aligned} \quad (15)$$

The correlation function of the environment $C(\tau)$ is defined as

$$C(\tau) = \Lambda^2 \sum_{\alpha\beta} [1 - f(\varepsilon_\alpha)] f(\varepsilon_\beta) |d_{\alpha\beta}|^2 e^{i\omega_{\alpha\beta}\tau}, \quad (16)$$

and contains the relevant information on the time evolution of the relative-coordinate degrees of freedom. In (16), $f(\varepsilon) = [e^{\beta(\varepsilon-\mu)} + 1]^{-1}$ is the Fermi function and $\omega_{\alpha\beta} = (\varepsilon_\alpha - \varepsilon_\beta)/\hbar$.

For not too small nanoparticles, the electronic environment described by the Hamiltonian (5) contains a large number of degrees of freedom, and its spectrum is therefore quasi-continuous. Thus, the exponentials contributing to the correlation function (16) very efficiently suppress the sum for not too small τ . Indeed, for zero temperature it is shown in [17] that the typical correlation time $\langle\tau_{\text{cor}}\rangle$ of the environment in terms of the surface plasmon relaxation time τ_{pl} is given by $\langle\tau_{\text{cor}}\rangle/\tau_{\text{pl}} \approx (k_{\text{F}}a)^{-1}$, where k_{F} is the Fermi wavevector. For nanoparticles with a radius larger than approximately 1 nm, one typically finds τ_{pl} to be of the order of or larger than $10\langle\tau_{\text{cor}}\rangle$. The effect of finite temperatures on this estimate is expected to be weak [13].

For sufficiently large nanoparticles, we can therefore work within the Markov approximation [14], where the density matrix ρ in (15) can be assumed to vary on much longer timescales than the decay time of the correlation function $C(t)$. The integral in (15) can then be carried out. After returning to the Schrödinger picture, and within the secular approximation [14], where highly oscillating terms are neglected, we finally obtain the master equation for the reduced density matrix of the centre-of-mass degree of freedom in the absence of the external driving field

$$\begin{aligned} \dot{\rho}(t) = & -i\omega_{\text{sp}} [b^\dagger b, \rho(t)] \\ & - \frac{\gamma_-}{2} [b^\dagger b \rho(t) + \rho(t) b^\dagger b - 2b\rho(t)b^\dagger] \\ & - \frac{\gamma_+}{2} [bb^\dagger \rho(t) + \rho(t) bb^\dagger - 2b^\dagger \rho(t)b]. \end{aligned} \quad (17)$$

Here, we have defined

$$\gamma_{\pm} = \frac{2\pi}{\hbar^2} \Lambda^2 \sum_{\alpha\beta} [1 - f(\varepsilon_\alpha)] f(\varepsilon_\beta) |d_{\alpha\beta}|^2 \delta(\tilde{\omega}_{\text{M}} \pm \omega_{\alpha\beta}), \quad (18)$$

while the renormalised surface plasmon frequency reads

$$\omega_{\text{sp}} = \tilde{\omega}_{\text{M}} - \delta \quad (19)$$

with

$$\delta = \frac{2}{\hbar^2} \Lambda^2 \mathcal{P} \sum_{\alpha\beta} [1 - f(\varepsilon_\alpha)] f(\varepsilon_\beta) |d_{\alpha\beta}|^2 \frac{\omega_{\alpha\beta}}{\omega_{\alpha\beta}^2 - \tilde{\omega}_{\text{M}}^2}, \quad (20)$$

where \mathcal{P} denotes the Cauchy principal value.

The expressions for γ_{\pm} and δ entering (17) have simple physical interpretations [13]: using Fermi's golden rule, γ_+ and γ_- are related to the lifetime $\tau_n = \gamma_n^{-1}$ of the n th excited state of the harmonic oscillator describing the centre-of-mass system by

$$\gamma_n = n\gamma_- + (n+1)\gamma_+, \quad (21)$$

while δ is the frequency shift due to the interaction of the system with the electronic environment. As the surface plasmon corresponds to the first excited state of the harmonic oscillator, its lifetime is given by $\tau_{\text{pl}} = \gamma_1^{-1}$. We have evaluated these important and experimentally relevant quantities in references [12,13] as a function of the size and temperature of the nanoparticle. The shift δ is positive, and thus we have a redshift of the surface plasmon frequency in addition to the redshift induced by the spill-out effect described by (4). This redshift of the surface plasmon frequency is due to the coupling of the centre-of-mass system to the electronic environment. It is analogous to the Lamb shift known in atomic physics [14,19].

3.2 Effect of the laser

We now consider the role of an external driving field whose interaction with the centre-of-mass coordinate is described by the time-dependent Hamiltonian $H_F(t)$ defined by (7). In a first step, we neglect the coupling Hamiltonian H_c between the centre of mass and the electronic environment during the excitation process. Thus, we do not have any relaxation mechanism for the surface plasmon excitation, and its frequency (19) remains unrenormalised. As a consequence, we have

$$\dot{\rho}(t) = -i\tilde{\omega}_M [b^\dagger b, \rho(t)] - i\Omega_R \cos(\omega_L t) [b^\dagger + b, \rho(t)] \quad (22)$$

which describes the standard time evolution of a harmonic oscillator driven by an external monochromatic field.

Assuming that the driving does not influence the dissipation of the surface plasmon excitation, we can add the contributions from H_c , i.e., the dissipative part of the reduced density matrix described by the master equation (17), and from $H_F(t)$ (see Eq. (22)) independently. This is justified provided that the memory time of the environment $\langle \tau_{\text{cor}} \rangle$ is much smaller than Ω_R^{-1} which is determined by the coupling to the driving field [14]. The matrix representation of the master equation in the harmonic oscillator basis is then that of a driven damped harmonic oscillator,

$$\begin{aligned} \dot{\rho}_{nm} = & -i\omega_{\text{sp}}(n-m)\rho_{nm} \\ & -\gamma \left(\frac{n+m}{2}\rho_{nm} - \sqrt{(n+1)(m+1)}\rho_{n+1,m+1} \right) \\ & -i\Omega_R \cos(\omega_L t) \left(\sqrt{n}\rho_{n-1,m} + \sqrt{n+1}\rho_{n+1,m} \right. \\ & \left. - \sqrt{m}\rho_{n,m-1} - \sqrt{m+1}\rho_{n,m+1} \right). \end{aligned} \quad (23)$$

In this equation, we have neglected γ_+ as compared to γ_- and set $\gamma = \gamma_-$ which corresponds to the Landau damping linewidth. Indeed, it is easy to show from (18) that the rate γ_+ is related to γ_- through the detailed-balance relation $\gamma_+ = e^{-\beta\hbar\tilde{\omega}_M}\gamma_-$. We have $\gamma_+ \ll \gamma_-$ for temperatures up to a few thousand degrees since $\hbar\tilde{\omega}_M$ is of the order of several eV.

4 Two-level system approach

In order to obtain from (23) the time evolution of the centre-of-mass degree of freedom under the influence of the external driving field and the coupling to the relative-coordinate system, it is useful to introduce an appropriate simplification. The centre-of-mass system, which has been modelled as a harmonic oscillator described by the Hamiltonian (3), can be truncated to a two-level system. The applicability of such an approximation is discussed in the appendix but can be motivated as follows: Except for a very strong driving field, the harmonic oscillator states above the first excited state are not significantly populated. Furthermore, the detuning between the frequency of the laser and the resonance frequency of the system plays in favour of the two-level description. Moreover, there exist additional damping mechanisms which are not included in our model which tend to depopulate the higher states, like the ionisation of an electron via the double-plasmon state [12] or the radiation damping [2]. In the case of pump-probe experiments on noble-metal nanoparticles embedded in a dielectric medium, interactions with the surrounding matrix provide further decay channels, e.g. via coupling to phonons, localised states, surface states, etc. As the second collective level, the so-called double plasmon, has a width which is significantly larger than the one of the simple surface plasmon, it is justified to neglect all excited levels but the first one. In addition, the double-plasmon state has not been clearly identified experimentally, even though indirect observations of such a state have been reported in experiments on charged sodium clusters in vacuum [20].

Writing the master equation (23) for the two collective states $|0\rangle$ and $|1\rangle$, introducing the new variables

$$\hat{\rho}_{nm} = \rho_{nm} e^{i\omega_L(n-m)t} \quad (24)$$

and keeping only the terms which significantly contribute close to the resonance $\omega_L \approx \omega_{\text{sp}}$ (rotating wave approximation [14]), one obtains

$$\dot{\hat{\rho}}_{11} = i\frac{\Omega_R}{2} (\hat{\rho}_{10} - \hat{\rho}_{01}) - \gamma\hat{\rho}_{11}, \quad (25a)$$

$$\dot{\hat{\rho}}_{01} = -i\delta_L\hat{\rho}_{01} - i\frac{\Omega_R}{2} (\hat{\rho}_{11} - \hat{\rho}_{00}) - \frac{\gamma}{2}\hat{\rho}_{01}. \quad (25b)$$

Here, $\delta_L = \omega_L - \omega_{\text{sp}}$ is the detuning between the laser and the resonance frequency, and we have the conditions $\hat{\rho}_{00} + \hat{\rho}_{11} = 1$ and $\hat{\rho}_{10}^* = \hat{\rho}_{01}$. It is often useful to define a scaled detuning $\Delta = \delta_L/\gamma$ and the saturation parameter

$$s = 2 \left(\frac{\Omega_R}{\gamma} \right)^2 \quad (26)$$

which is a measure of the ratio between the field intensity and the damping strength. As a function of these parameters, whose experimentally relevant values are discussed in the next section, the stationary solutions of the Bloch

equations (25) are [14]

$$\rho_{11}^{\text{st}} = \frac{s}{2(1+s+4\Delta^2)}, \quad (27)$$

$$\rho_{01}^{\text{st}}(t) = e^{i\omega_L t} \frac{2\Delta + i}{1+s+4\Delta^2} \left(\frac{s}{2}\right)^{1/2}. \quad (28)$$

The occupation probability ρ_{11}^{st} of the first excited state of the centre-of-mass system increases with increasing saturation parameter s and decreases with increasing detuning Δ between the frequency of the laser field ω_L and the resonance frequency ω_{sp} . The coherence ρ_{01} determines the mean centre-of-mass coordinate according to $\langle Z \rangle = 2\ell \text{Re}(\rho_{01})$ where ℓ has been defined in (9). The amplitude of the oscillation of $\langle Z \rangle$ increases with increasing s up to $s = 1 + 4\Delta^2$, while it decreases for larger s and approaches zero in the limit of infinite s .

For zero detuning, $\delta_L = 0$, (25) can be solved analytically. Assuming that the system is initially in its ground state, $\rho(0) = |0\rangle\langle 0|$, the full time dependence of the density matrix is determined by [21]

$$\rho_{11}(t) = \frac{s}{2(1+s)} \left\{ 1 - e^{-3\gamma t/4} \left[\cosh\left(\frac{\gamma t}{4}\sqrt{1-8s}\right) + \frac{3}{\sqrt{1-8s}} \sinh\left(\frac{\gamma t}{4}\sqrt{1-8s}\right) \right] \right\} \quad (29)$$

for the population of the excited state, and

$$\rho_{01}(t) = \frac{i e^{i\omega_{\text{sp}} t}}{1+s} \left(\frac{s}{2}\right)^{1/2} \left\{ 1 - e^{-3\gamma t/4} \left[\cosh\left(\frac{\gamma t}{4}\sqrt{1-8s}\right) + \frac{1-2s}{\sqrt{1-8s}} \sinh\left(\frac{\gamma t}{4}\sqrt{1-8s}\right) \right] \right\} \quad (30)$$

for the coherence.

Figure 1a shows the population (29) of the excited state ρ_{11} as a function of time for various values of the saturation parameter and without detuning ($\delta_L = 0$). For $s \leq 1/8$, ρ_{11} monotonically increases as a function of time to reach the stationary value given in (27). For $s > 1/8$, the centre-of-mass system exhibits damped Rabi oscillations and reaches the steady state on the timescale $\sim \gamma^{-1}$. If the laser field is turned off after a certain time τ , the population of the excited state relaxes to zero according to

$$\rho_{11}(t) = \rho_{11}(\tau) e^{-\gamma(t-\tau)}, \quad (31)$$

while the coherence of the system decays as

$$\rho_{01}(t) = \rho_{01}(\tau) e^{-(\gamma/2 - i\omega_{\text{sp}})(t-\tau)}. \quad (32)$$

One can see in Figure 1 that even for a strong saturation parameter, the steady state regime is reached for times $t \lesssim 8\gamma^{-1}$.

In Figure 1b, we show the mean centre-of-mass position $\langle Z \rangle$ as a function of time. For $s \ll 1$, $\langle Z \rangle$ oscillates regularly, while its amplitude increases monotonically as a function of time. In the case of strong saturation parameter $s \gg 1$, it is clear from (30) that the dynamics of the centre of mass is determined by the beating between the two oscillating contributions at the frequencies ω_{sp} and Ω_R for times shorter than a few γ^{-1} (see the solid line in Fig. 1b).

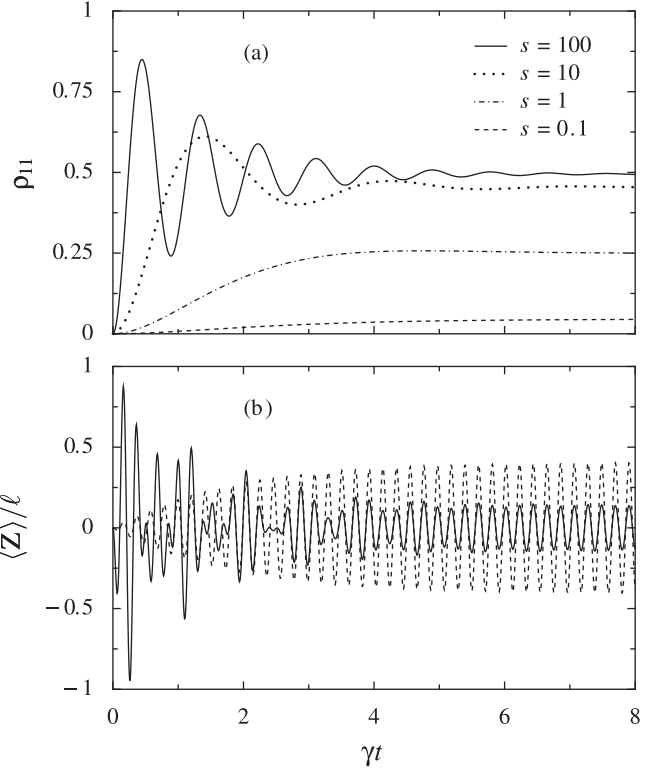


Fig. 1. (a) Population of the excited state ρ_{11} (29) as a function of γt for different values of the saturation parameter s and for $\delta_L = 0$. (b) Mean centre-of-mass coordinate $\langle Z \rangle$ for $s = 0.1$ and 100. In the figure, $\omega_{\text{sp}}/\gamma = 30$ and $\delta_L = 0$.

5 Saturation parameter

The results in the previous section show that the saturation parameter (26) is decisive for the dynamics of the surface plasmon excitation in the presence of an external driving field. In typical photoabsorption experiments [1], a weak laser field excites an ensemble of nanoparticles. For a laser power of a few mW, the resulting electric field is of the order of 10^3 V m^{-1} , and thus the Rabi frequency (8) is no more than several μeV . The order of magnitude of the surface plasmon linewidth in metallic nanoparticles is 100 meV, so that one finds $s \ll 1$. In that case we are in the linear-response regime, i.e., the power absorbed by the nanoparticle is proportional to the intensity of the laser.

On the contrary, in pump-probe experiments, the nanoparticles are excited by an ultrashort pump laser pulse of high intensity. As a typical example, we consider the experiments of [7] on silver nanoparticles with an average radius $a = 3.25 \text{ nm}$ embedded in a glass matrix. These nanoparticles present a broad absorption spectrum around the resonance frequency $\omega_{\text{sp}} = 2.85 \text{ eV}$. According to time-dependent local density approximation calculations [12], the width of this resonance is approximately $\gamma = 50 \text{ meV}$. The estimation of the Rabi frequency (8) requires the knowledge of the electrical field E_0 of the laser. This quantity can be inferred from the energy $\bar{u} = \epsilon_0 \epsilon_r E_0^2 c \tau / 2$ of a laser pulse divided by its cross section [7], where c is the speed of light, ϵ_0 the vacuum permittivity, $\epsilon_r \simeq 6$ for glass,

and τ the duration of the pulse (typically 100 fs). With $\bar{u} = 1 \text{ J m}^{-2}$, one finds $E_0 = 3.6 \times 10^7 \text{ V m}^{-1}$. The Rabi frequency is therefore $\Omega_R \simeq 0.38 \text{ eV}$, which results in a very large saturation parameter $s \simeq 100$. Thus we are far beyond the linear-response regime. Notice that the duration of the pump-laser pulse considered here corresponds to $\gamma\tau \simeq 8$. Thus, according to Figure 1, even for ultrashort laser pulses the centre of mass can reach its steady state before the end of the pulse.

6 Absorption spectrum of a weak probe beam

As it is shown in the appendix, the dynamics of the surface plasmon is well described by a two-level system driven by an external field and damped by its coupling to the electronic environment. This is reminiscent of the well-known situation in quantum optics, where a transition between two levels of an atom is excited by a strong laser. The concept of dressed levels [14,22], arising as coherent superpositions of atom-photon states has proven to be very useful to describe the coupled system, in particular when the driving is strong as compared to the damping. In the presence of a small detuning δ_L between the pump laser field and the transition frequency of the two-level system, the absorption spectrum of a second laser acting as a weak probe contains sidebands. Interestingly, in one of the sidebands the probe beam is damped by absorption processes, while stimulated emission processes amplify the probe beam in the other sideband. This phenomenon has been observed experimentally for different driven systems. Examples include the case of an optical transition in sodium atoms [23] and a nuclear magnetic hyperfine transition of a nitrogen-vacancy centre in diamond [24].

In the present paper we focus on a surface plasmon excitation driven by a strong laser field. This is a completely analogous situation since the dynamics of the surface plasmon can be described by an effective two-level system with a transition energy $\hbar\omega_{\text{sp}}$, coupled to a pump laser with frequency ω_L . Without coupling ($\Omega_R = 0$), the basis states are $|0, N_p + 1\rangle$ and $|1, N_p\rangle$ representing the plasmon in its ground and excited state with $N_p + 1$ and N_p photons in the pump laser field, respectively. The energy difference between those states is given by the detuning $\hbar\delta_L = \hbar(\omega_L - \omega_{\text{sp}})$ of the pump laser with respect to the plasmon transition. The coupling by H_F (Eq. (7)) leads to a mixing of the basis states, giving rise to the dressed plasmon levels with an energy splitting $\hbar\Omega = \hbar\sqrt{\Omega_R^2 + \delta_L^2}$, where Ω_R is the Rabi frequency (8). The dressed plasmon levels $|A(N_p)\rangle$ and $|B(N_p)\rangle$ arise as superpositions of the uncoupled basis states $|0, N_p + 1\rangle$ and $|1, N_p\rangle$ referring to different photon numbers. In this doublet, we denote the upper and lower dressed level by $|A(N_p)\rangle$ and $|B(N_p)\rangle$, respectively.

Four optical transitions (see thick arrows in Fig. 2) are allowed between dressed states corresponding to neighbouring photon numbers because of the mixture of those states with the ones of the uncoupled basis. Since the stationary populations of $|A(N_p)\rangle$ and $|B(N_p)\rangle$ are to a very

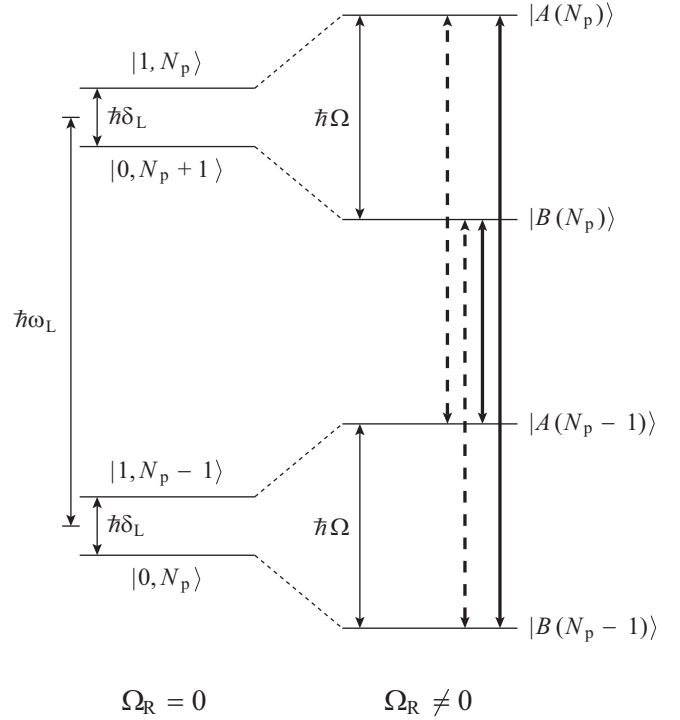


Fig. 2. Scheme of the uncoupled ($\Omega_R = 0$) and dressed states ($\Omega_R \neq 0$). The four allowed optical transitions are indicated by vertical thick arrows. See the text for details.

good approximation independent of N_p , there is no peak in the absorption spectrum of the weak probe beam at the frequency ω_L (see the two thick dashed arrows in Fig. 2).

For $\delta_L > 0$, the upper dressed levels $|A(N_p)\rangle$ have a higher stationary population than the lower ones $|B(N_p)\rangle$. Therefore, a population inversion appears in the transition $|A(N_p)\rangle \leftrightarrow |B(N_p - 1)\rangle$. This leads to a sideband at the frequency $\omega_L + \Omega$ where the probe beam is amplified by stimulated emission. For the transition $|B(N_p)\rangle \leftrightarrow |A(N_p - 1)\rangle$ the lower state has the higher population such that the sideband at frequency $\omega_L - \Omega$ is of absorbing character. For negative detuning $\delta_L < 0$, when the pump laser frequency is below the bare transition energy, the populations of the dressed states are inverted. Now, the populations of the upper dressed levels $|A(N_p)\rangle$ are lower than the populations of the lower levels. In this case, the sideband at the frequency $\omega_L + \Omega$ is absorbing while the probe beam is expected to be amplified around the frequency $\omega_L - \Omega$.

The width of the sidebands is of the order of γ . In the so-called secular limit $\Omega \gg \gamma$, the sidebands are therefore well resolved and should be observable experimentally. Within this limit, it is straightforward to calculate the stationary populations of the dressed states [22]. For the case of a resonant pump laser $\delta_L = 0$, all the dressed states have the same populations. Therefore, to zero order in γ/Ω , the transitions do not influence the probe beam. A more detailed discussion beyond the parameter regimes considered here is given e.g. in references [23,25].

An experimental observation of the sidebands should be feasible using an intense pump laser with $s \simeq 100$ and

a pulse duration longer than 100 fs. Then, the frequency width of the pump pulse is below 0.01 eV, which allows to adjust the detuning δ_L with high precision. With the Rabi frequency $\Omega_R \simeq 0.38$ eV and the linewidth $\gamma = 50$ meV estimated in Section 5 for the experiments of reference [7], one should be able to observe well resolved sidebands.

7 Conclusion

Using standard methods of quantum optics, we have studied the dynamics of the surface plasmon in metallic nanoparticles driven by an electrical field. Decoherence and dissipation occur due to the coupling of the collective excitation to the electronic environment constituted by particle-hole pairs. Exploiting the Markovian character of the environment [17], we have established the master equation for the surface plasmon density matrix.

We have shown that for realistic experimental situations, a model taking into account only the two lowest levels is sufficient to describe the dynamics of the collective degree of freedom. This allows to consider a large variety of experimentally relevant situations, from photoabsorption to pump-probe setups.

Motivated by the analogy to quantum optics, we have introduced collective states that are dressed by the photons of the pump laser. We predict that for strong driving, the dressed states will manifest themselves through the appearance of sidebands in the absorption spectrum of a weak probe laser. Depending on the detuning of the pump laser, these spectral features have absorbing or amplifying character and their position relative to the pump frequency is determined by the pump intensity. Although these sidebands have so far not been observed in metallic nanoparticles, their detection should be feasible with modern experimental techniques, thereby offering access to dressed surface plasmon states.

We thank S. Kohler for useful discussions. We acknowledge financial support from DAAD and Égide through the Procope program, from the BFHZ-CCUFB and from the European Union within the MCRTN program. G.W. thanks the Deutsche Forschungsgemeinschaft for financial support during the final phase of this work.

Appendix A: Three-level system

In this appendix we discuss the validity of a two-level approach for the description of the centre-of-mass system, whose Hamiltonian is given in (3). For this purpose, we consider a three-level system and study the conditions under which its description can be safely reduced to that of a two-level system. A phenomenological master equation description of the plasmon in terms of three levels has been discussed by Liau et al. [26]. In that case, however, three levels were required to describe two-photon processes in two-pulse second-order interferometry.

According to (21), the Landau damping linewidth for the second level of the harmonic oscillator at zero temperature is 2γ , where γ is the width of the first excited state [12, 27]. In addition, two more mechanisms contribute to the damping of the second level: (i) first order processes which lead to the decay into the first level (like the radiation damping [1, 2] or the coupling to the surrounding matrix [27]); (ii) second-order processes which result in the direct decay into the ground state (like the ionisation [12]). We denote the damping rates associated with these two additional channels by γ_1 and γ_2 , respectively.

Within the Lindblad theory [28], these channels are accounted for by adding

$$\langle n| \sum_{a=1,2} \frac{\gamma_a}{2} (2L_a \rho L_a^\dagger - L_a^\dagger L_a \rho - \rho L_a^\dagger L_a) |m\rangle \quad (33)$$

to the right-hand side of the master equation (23). We choose the Lindblad operators as $L_1 = |1\rangle\langle 2|$ and $L_2 = |0\rangle\langle 2|$, which lead to transitions between the centre-of-mass states $|2\rangle$ and $|1\rangle$, and $|2\rangle$ and $|0\rangle$, respectively. The rotating-wave approximation then yields the following set of coupled differential equations

$$\begin{aligned} \dot{\hat{\rho}}_{00} &= -i \frac{\Omega_R}{2} (\hat{\rho}_{10} - \hat{\rho}_{01}) + \gamma \hat{\rho}_{11} + \gamma_2 \hat{\rho}_{22}, \\ \dot{\hat{\rho}}_{22} &= -i \frac{\Omega_R}{2} \sqrt{2} (\hat{\rho}_{12} - \hat{\rho}_{21}) - \left(2\gamma + \sum_{a=1,2} \gamma_a \right) \hat{\rho}_{22}, \\ \dot{\hat{\rho}}_{01} &= -i \delta_L \hat{\rho}_{01} - i \frac{\Omega_R}{2} (\hat{\rho}_{11} - \hat{\rho}_{00} - \sqrt{2} \hat{\rho}_{02}) \\ &\quad - \frac{\gamma}{2} \hat{\rho}_{01} + \sqrt{2} \gamma \hat{\rho}_{12}, \\ \dot{\hat{\rho}}_{12} &= -i \delta_L \hat{\rho}_{12} - i \frac{\Omega_R}{2} [\hat{\rho}_{02} + \sqrt{2} (\hat{\rho}_{22} - \hat{\rho}_{11})] \\ &\quad - \frac{1}{2} \left(3\gamma + \sum_{a=1,2} \gamma_a \right) \hat{\rho}_{12}, \\ \dot{\hat{\rho}}_{02} &= -2i \delta_L \hat{\rho}_{02} - i \frac{\Omega_R}{2} (\hat{\rho}_{12} - \sqrt{2} \hat{\rho}_{01}) \\ &\quad - \frac{1}{2} \left(2\gamma + \sum_{a=1,2} \gamma_a \right) \hat{\rho}_{02}. \end{aligned} \quad (34)$$

In order to obtain quantitative results, the two additional damping constants in the following are assumed to be equal, i.e., $\gamma_1 = \gamma_2 = \gamma_{\text{add}}$. Figure 3 presents the stationary solution of (34) for the population of the second excited state ρ_{22}^{st} as a function of γ_{add} for different values of the detuning $\Delta = \delta_L/\gamma$ and a large saturation parameter $s = 100$. It can be seen that for $\Delta \gtrsim 5$, which corresponds to the typical detuning in the pump-probe experiments of reference [7], the probability to find the second collective state occupied is less than 10% and is almost constant as a function γ_{add} . In the case $\Delta < 5$, ρ_{22}^{st} decreases with γ_{add} but may be non-negligible. In this case, the assumption of a two-level system to describe the surface plasmon dynamics might be questionable.

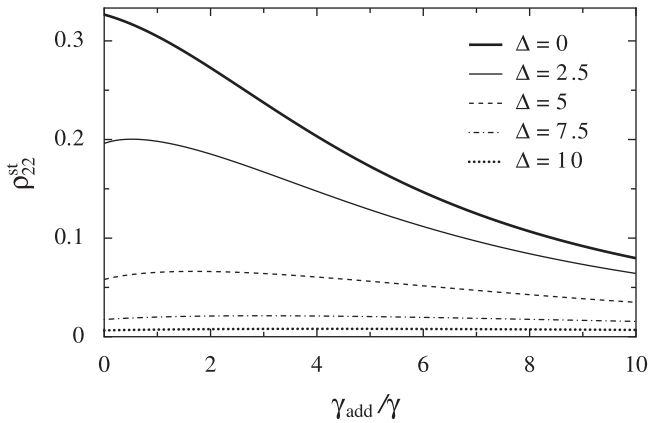


Fig. 3. Stationary solution of (34) for the population of the second excited state as a function of the additional damping constant γ_{add} and for various values of the detuning Δ . In the figure, the saturation parameter is $s = 100$.

For a rather small saturation parameter, i.e., for a weak external laser field, the second collective state can be neglected for the description of the surface plasmon dynamics. In the case of a large saturation parameter, as it is for example the case in pump-probe experiments, this second collective state can be neglected for not too small detuning between the frequency of the pump laser and the resonance frequency.

References

1. W.A. de Heer, *Rev. Mod. Phys.* **65**, 611 (1993)
2. M. Brack, *Rev. Mod. Phys.* **65**, 677 (1993)
3. T. Tokizaki, A. Nakamura, S. Kaneko, K. Uchida, S. Omi, H. Tanji, Y. Asahara, *Appl. Phys. Lett.* **65**, 941 (1994)
4. J.-Y. Bigot, J.-C. Merle, O. Cregut, A. Daunois, *Phys. Rev. Lett.* **75**, 4702 (1995)
5. M. Perner, P. Bost, U. Lemmer, G. von Plessen, J. Feldmann, U. Becker, M. Mennig, M. Schmitt, H. Schmidt, *Phys. Rev. Lett.* **78**, 2192 (1997)
6. V. Halté, J. Guille, J.-C. Merle, I. Perakis, J.-Y. Bigot, *Phys. Rev. B* **60**, 11738 (1999)
7. J.-Y. Bigot, V. Halté, J.-C. Merle, A. Daunois, *Chem. Phys.* **251**, 181 (2000)
8. N. Del Fatti, F. Vallée, C. Flytzanis, Y. Hamanaka, A. Nakamura, *Chem. Phys.* **251**, 215 (2000)
9. C. Voisin, N. Del Fatti, D. Christofilos, F. Vallée, *J. Phys. Chem. B* **105**, 2264 (2001)
10. G. Weick, D. Weinmann, G.-L. Ingold, R.A. Jalabert, *Europhys. Lett.* **78**, 27002 (2007)
11. L.G. Gerchikov, C. Guet, A.N. Ipatov, *Phys. Rev. A* **66**, 053202 (2002)
12. G. Weick, R.A. Molina, D. Weinmann, R.A. Jalabert, *Phys. Rev. B* **72**, 115410 (2005)
13. G. Weick, G.-L. Ingold, R.A. Jalabert, D. Weinmann, *Phys. Rev. B* **74**, 165421 (2006)
14. C. Cohen-Tannoudji, J. Dupont-Roc, G. Grynberg, *Atom-photon interactions: Basic processes and applications* (Wiley-VCH, New York, 1992)
15. K. Hagino, *Phys. Rev. B* **60**, R2197 (1999)
16. C. Yannouleas, R.A. Broglia, *Ann. Phys. (N.Y.)* **217**, 105 (1992)
17. C. Seoanez, G. Weick, R.A. Jalabert, D. Weinmann, *Eur. Phys. J. D* **44**, 351 (2007)
18. See, e.g., U. Weiss, *Quantum Dissipative Systems* (World Scientific, Singapore, 1993) which can also serve as a guide to the recent literature in this field
19. W.E. Lamb, R.C. Retherford, *Phys. Rev.* **72**, 241 (1947); W.E. Lamb, *Rep. Prog. Phys.* **14**, 19 (1951)
20. R. Schlipper, R. Kusche, B. von Issendorff, H. Haberland, *Phys. Rev. Lett.* **80**, 1194 (1998); R. Schlipper, R. Kusche, B. von Issendorff, H. Haberland, *Appl. Phys. A: Mater. Sci. Process.* **72**, 255 (2001)
21. D.F. Walls, G.J. Milburn, *Quantum Optics* (Springer-Verlag, Berlin, 1994)
22. C. Cohen-Tannoudji, S. Reynaud, *J. Phys. B: At. Mol. Phys.* **10**, 345 (1977); C. Cohen-Tannoudji, S. Reynaud, in: *Proc. Int. Conf. on Multiphoton Processes*, edited by J.H. Eberly, P. Lambropoulos (Wiley, New York, 1978), p. 103
23. F.Y. Wu, S. Ezekiel, M. Ducloy, B.R. Mollow, *Phys. Rev. Lett.* **38**, 1077 (1977)
24. C. Wei, N.B. Manson, *Phys. Rev. A* **49**, 4751 (1994)
25. B.R. Mollow, *Phys. Rev. A* **5**, 2217 (1972)
26. Y.-H. Liau, A.N. Unterreiner, Q. Chang, N.F. Scherer, *J. Phys. Chem. B*, **105**, 2135 (2001)
27. R.A. Molina, D. Weinmann, R.A. Jalabert, *Phys. Rev. B* **65**, 155427 (2002); R.A. Molina, D. Weinmann, R.A. Jalabert, *Eur. Phys. J. D* **24**, 127 (2003)
28. G. Lindblad, *Commun. Math. Phys.* **48**, 119 (1976); V. Gorini, A. Kossakowski, E.C.G. Sudarshan, *J. Math. Phys.* **17**, 821 (1976)